Received XX Month, XXXX; revised XX Month, XXXX; accepted XX Month, XXXX; Date of publication XX Month, XXXX; date of current version XX Month, XXXX.

Digital Object Identifier 10.1109/XXXX.2022.1234567

Physics of Phase Transition Switches

Muhammad Ashraful Alam[1], Fellow, IEEE, Nicolò Zagni[2], Member, IEEE

[1]School of Electrical and Computer Engineering (ECE), Purdue University, West Lafayette, IN 47907 USA
[2]Department of Engineering "Enzo Ferrari," University of Modena and Reggio Emilia, 41125 Modena, Italy

(Invited Paper)

Corresponding author: M. A. Alam (email: alam@ purdue.edu).

ABSTRACT The semiconductor industry is undergoing an epochal shift, driven by the move to pseudo-three- (2.5D) and three-dimensional (3D) packaging of integrated circuits based on non-scalable classical Boltzmann transistors. In this regard, the scaling potential of post-Boltzmann phase-transition logic switches, memory elements, super-Nernstian sensors, and zero-energy displays remains underappreciated. Broadly defined, phase-transition switches operate between two stable states separated by an energy or power barrier, offering promising solutions for the future of electronics. This tutorial paper provides a foundational and intuitive understanding of the emerging field of phase-transition electronics. It also highlights open issues and research opportunities, serving as a roadmap for advancing this critical technology.

INDEX TERMS Beyond CMOS, Boltzmann Tyranny, Double-Well Energy Landscape, Ferroelectric, Negative Capacitance, NEMS, Phase Transition.

I. INTRODUCTION

Over the last 125 years, the four core functions of information processing – logic, memory, sensing, and display – have been supported by three generations of device technologies: vacuum tubes, bipolar transistors, and metal-oxide-semiconductor field-effect transistors (MOSFETs). Despite their different applications, whether in digital logic (MOSFETs), data storage (Flash memory), displays (LEDs), or biosensing (ion-sensitive switches), these Boltzmann switches share a fundamental reliance on the controlled injection of Boltzmann-distributed electrons over an electrostatically controlled energy barrier, created by different combinations of metallic/semiconducting/insulating materials. There is a broad consensus that we have approached the scaling limits of these classical devices for complementary metal-oxide-semiconductor technology (CMOS), and the focus must now shift toward 2.5D and 3D integration of non-scalable Boltzmann transistors [1].

Since the 1960s, we have seen scattered reports on devices that rely on the principle of phase transition (PT) to create alternative solutions for the aforementioned four fundamental functions of logic, memory, sensing, and d isplay [2], [3], see Table 1. These phase-transition switches include bistable ferroelectric field-effective transistors, negative capacitance transistors [4], [5], nano electro-mechanical system (NEMS) switches [6], [7], atomic switch [8], correlated electron devices [9], electrophoretic and other bistable passive displays [10]–[12], bifurcation-based chemical and biosensors [13]–[15], etc. Indeed, classical devices, such as semiconductor lasers, static random access memory (SRAM), thyristors, impact-ionization FETs, etc. also rely on the principles of (power) PT. Could this new class of phase transition devices collectively define the next generation of scalable electronic components?

Unlike Boltzmann switches, PT transistors rely on an energy landscape with two stable states separated by an energy barrier. This energy landscape offers three significant advantages. First, since the energy barrier can be formed within a single material, PT switches avoid the scaling limitations faced by Boltzmann switches (Boltzmann switches require a combination of materials to create the barrier). Second, PT switches are not constrained by the Boltzmann limit, enabling potentially lower-energy operation. Lastly, PT switches offer a much better signal-to-noise ratio (SNR), allowing for analog sensor performance that surpasses other technologies.

In this paper, we provide a tutorial and an integrated review of PT switches. The paper is structured as follows. In Section 2, we explain the physics of phase transitions using the example of a buckling stick, interpreted using phase-

TABLE 1. Until recently, Moore's law has relied on the scaling of Boltzmann switches. Although phase-transition switches also have a long-history, recent innovations have broaden potential applications in logic, memory, sensor, and display.

Year	Device	Principle	Application
1906 [16]	Vacuum Tube Triode	Boltzmann	Logic, oscillators
1927 [17]	LED	Boltzmann	Display
1948 [18]	Bipolar Transistor	Boltzmann	Logic, memory
1957 [19]	FeFET	Phase Transition	Memory
1959 [20]	MOSFET	Boltzmann	Logic, Memory
1970 [21]	ISFET	Boltzmann	Biosensors
1998 [22]	MottFET	Phase Transition	Logic
2002 [23]	SGFET	Phase Transition	Logic, Memory
2007 [24]	NEMFET[1]	Phase Transition	Logic, Memory
2008 [5]	NCFET	Phase Transition	Logic
2012 [13]	FlexureFET	Phase Transition	Biosensors
2015 [25]	PhaseFET[2]	Phase Transition	Logic, oscillator

[1] Nano-electro-mechanical FET.

[2] Also called Hyper FET.

transition terminology. Building on this conceptual framework, Section 3 explores the performance of various devices, including NEMS capacitors, negative capacitance transistors (NCFETs), ferroelectric transistor memories (FeFETs), and nanobiosensors. Despite their apparent differences, these examples demonstrate that all phase-transition switches share common operating principles and can be analyzed within a unified framework. Section 4 summarizes our conclusions. The paper assumes that the readers are familiar with the classical physics of MOSFET. For completeness, the subthreshold slope of a MOSFET and related metrics are summarized in the appendix.

II. A Tutorial Introduction to Phase Transition Physics

The phenomenon of phase transition is characterized by an abrupt (and often discontinuous) transformation of a physical system from one state to another. The state of the system can be defined as the specific pattern of organization displayed by the system itself, characterized by its "order parameter." For instance, PT occurs when matter transforms from liquid to solid or gas, which modifies the arrangement of atoms from a solid crystal to a random pattern in a fluid phase. The order parameter is the density difference between the phases. This transition is reversible, allowing repeated switching between states [26].

The theory of phase transition defines a crowning success of condensed matter physics, and the complex mathematics makes the topic mysterious and its relevance to modern semiconductor devices difficult to understand. In the following discussion, we will begin with a simple pedagogical discussion of the phase transition. We will then use this theory (Landau) to explain the opportunities and challenges of phase-transition switches and sensors.

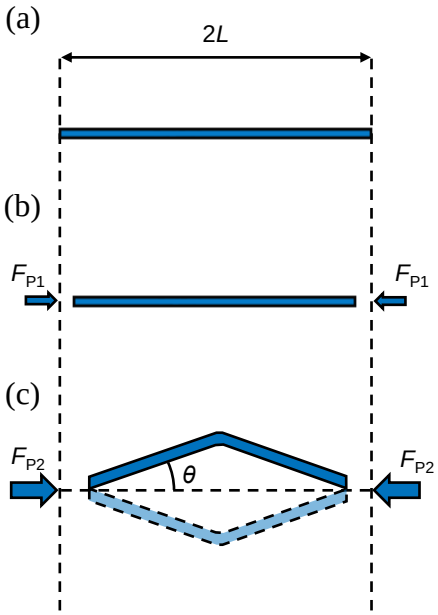

FIGURE 1. (a) Stick of total length $2L$ in rest position. (b) A small pressure F_{P1} is applied from both sides, and the stick compresses linearly. (c) The applied pressure F_{P2} exceeds a certain critical value $F_{\mathrm{P,C}}$, hence the stick buckles and becomes unstable. The angle it forms with respect to the rest position is labeled as θ.

A. Buckling of a stick as a model of phase transtion

This simple example introduces the essence of instability and illustrates (second order) PT. Consider the system shown in Fig. 1(a) composed of a thin stick of length $2L$ placed at rest along a horizontal line. If we press from both ends of the stick, initially, the stick would compress linearly with the applied pressure, as in Fig. 1(b). Beyond a critical pressure, however, the stick suddenly buckles (i.e., assumes an arched shape), see Fig. 1(c). From this point onward, the deformed stick would continue to buckle. If pushed far enough, it will reach the breaking point and snap into two or more pieces.

The shape of the stick is determined by minimizing the energy input from the external force (U_{P}) and the restoring elastic energy of the stick (U_τ). The energy due to the external force is calculated by multiplying the force, F_p by the displacement of the stick, namely $\Delta L = 2L(1-\cos(\theta))$, so that i.e., $U_{\mathrm{P}} = 2F_{\mathrm{P}}L(1-\cos(\theta)) = 2F_{\mathrm{P}}L\sin^2(\theta/2)$. The restoring elastic energy is calculated by integrating the rotational torque ($\tau = -k_r\theta$) over the angle θ, i.e., $U_\tau = 2\times 1/2 k_\tau \theta^2$. Here, k_τ is the rotational spring constant, expressed in $\mathrm{Nm/rad}$. The factor of 2 accounts for the elastic energy for the two ends of the stick.

The total energy thus reads

$$\frac{U}{2} = \frac{U_\tau - U_{\mathrm{P}}}{2} = \frac{1}{2}k_\tau\theta^2 - 2F_{\mathrm{P}}L\sin^2\left(\frac{\theta}{2}\right). \qquad (1)$$

By convention the applied force is indicated with a negative sign, because the energy of the input source is supplied to the system.

Depending on the magnitude of the applied force, the energy is minimized either by linear compression of the stick

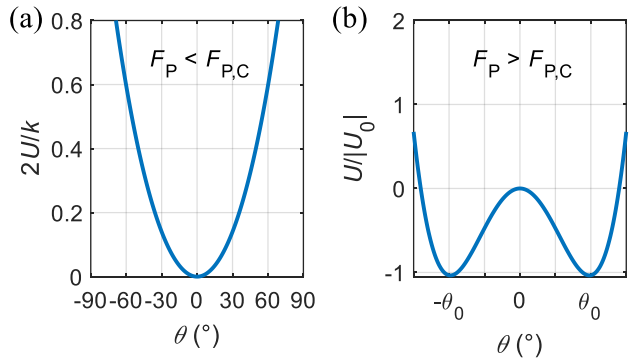

FIGURE 2. **Energy landscape $U - \theta$ of the buckling stick for (a) $F_P < F_{P,C}$ and (b) $F_P > F_{P,C}$. In (a) U is normalized by $k_\tau/2$, whereas in (b) it has been normalized by the energy minimum value $|U_0| = \alpha^2/(4\beta) \cdot (k/2)$.**

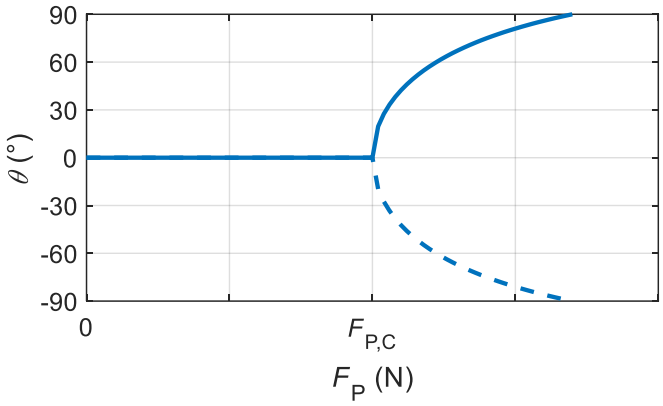

FIGURE 3. **θ vs. applied pressure (F_P) on the buckling stick. For $F_P < F_{P,C}$, $\theta = 0$, that is, the stick is unbuckled and compressed linearly in response to the applied pressure, F_P. For $F_P > F_{P,C}$, the stick buckles and θ diverge according to Eq. (4) (θ can be positive or negative depending on how "noise" present at the transition point.).**

or by bending it into an arched shape. This phase transition point is obtained by letting $\partial U/\partial\theta = 0$, i.e.,

$$\frac{F_P}{F_{P,C}} = \frac{\theta}{\sin(\theta)}, \tag{2}$$

where $F_{P,C} = k_\tau/L$ is the critical load.

B. Phase transition is described by a double-well energy landscape

For small θ, i.e., for $F_P < F_{P,C}$, $U(\theta)$ is minimized at the origin, i.e., $\theta = 0$, see Fig. 2(a). This result can be understood by considering that, below the critical force, the stick compresses but does not bend.

In contrast, for $F_P > F_{P,C}$, $U(\theta)$ develops a pair of energy minima (double-well) that can be obtained from the solution of Eq. (2), see Fig. 2(b). In this case, the beam buckles up (i.e., $\theta > 0$) or down ($\theta < 0$), and the symmetry of the system is broken, i.e., the system stabilizes itself randomly in one configuration or the other depending on the "random external perturbation" present in the system during the phase transition. These are the characteristic features of PT, where the change of the **order parameter** (in this case θ) leads to a sudden and macroscopic change in the behavior of the system.

Eq. (1) can be rewritten in a more compact form, i.e.,

$$\frac{U}{k_\tau} = \theta^2 - 2\frac{F_P}{F_{P,C}}(1 - \cos\theta) \approx \alpha\theta^2 + \beta\theta^4, \tag{3}$$

where $\alpha = (1 - F_P/F_{P,C})$ and $\beta = \frac{1}{12}F_P/F_{P,C}$. Eq. (3) is a general form of writing the energy of a PT system, that can be derived for different systems (this is discussed further in Section III).

Also, for $F_P > F_{P,C}$ the order parameter that minimizes energy can be written as

$$\theta = \pm\sqrt{6}\sqrt{1 - \frac{F_{P,C}}{F_P}} \approx \pm c(F_P - F_{P,C})^\delta, \tag{4}$$

with $c = \sqrt{6/F_P}$ and exponent $\delta = 0.5$. Eq. (4) is plotted in Fig. 3 (for $F_P = F_{P,C}$, $\theta = 0$). The power-law form of the order parameter as a function of the control parameter is also a common feature of systems undergoing phase transition. Observe that the order parameter, θ, varies continuously at the transition point, which is the typical behavior of second-order PT (first-order systems have an abrupt variation of the order parameter at the critical point [27]).

III. An integrative analysis of phase transition switches

In this section, we apply the elements of PT theory presented in Section II to interpret the behavior of different technologies, namely, NEMS capacitors, NCFETs, FeFETs, biosensors.

A. Phase transition in electro-mechanical NEMS Capacitor and Suspended-Gate MOSFET

While the buckling stick problem defines a purely mechanical PT, the **NEMS capacitor** defines the electro-mechanical PT. The NEMS capacitor is a simple integrated device composed of two electrodes separated by an air-gap, see Fig. 4. The bottom electrode is anchored and unmovable, while the upper one is supported by a spring and it is movable. In essence, this device is a capacitor with variable thickness air-gap. The air-gap is controlled by a voltage bias, V, applied through the movable upper electrode.

The function of NEMS is described by its $y - V$ (y is the displacement of the movable beam with respect to its rest position) and $V - Q$ (Q is the charge per unit area stored by the capacitor) relationships obtained from the balance of mechanical and electrical forces, namely [28],

$$y_*^3 - 2y_*^2 + y_* - M = 0 \tag{5a}$$

$$V = \alpha Q + \beta Q^3, \tag{5b}$$

where $y_* = y/y_0$, y_0 is the total air-gap thickness, $M = \varepsilon_0 A/(2ky_0^3)V^2$, ε_0 is vacuum dielectric constant, A is the cross-sectional area of the capacitor, k is the spring constant of the movable electrode, $\alpha = y_0/\varepsilon_0$, and $\beta = -A/(2k\varepsilon_0^2)$.

For this system, V is the control parameter and Q (or equivalently y_*) is the order parameter.

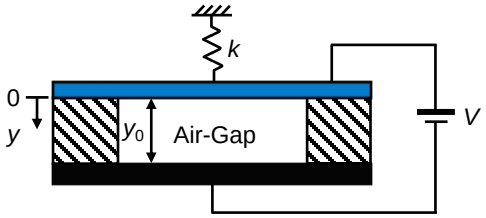

FIGURE 4. A schematic diagram of a NEMS capacitor. The height of the air-gap, $y(V) < y_0$ depends on the applied voltage V and the spring constant, k.

The total energy of the system (per unit area) is obtained as the sum of the mechanical and electrical one, namely

$$U = \frac{1}{2}\frac{k}{A}y^2 + \frac{1}{2}CV^2 - VQ, \tag{6}$$

where the first element on the right-hand side is the energy stored in the spring, the second one is the energy stored in the capacitor, $C = \varepsilon_0/(y_0 - y)$, and the last element is the energy drawn from the external battery. Minimization of Eq. (6) with respect to y is obtained when the mechanical and electrical forces balance each other out, occurring for $y = AQ^2/(2\varepsilon_0 k)$. In this case, Eq. (6) can be rewritten as follows,

$$U = \frac{1}{2}\alpha Q^2 + \frac{1}{4}\beta Q^4 - VQ, \tag{7}$$

which has a similar form as that of Eq. (3). Notice that Eq. (7) can also be obtained by integration of Eq. (5b) with respect to Q. The plot of $U - Q$ ($U - y_*$) and $y_* - V$ are shown in Fig. 5.

Although the form of Eq. (7) and Eq. (3) is similar, in the case of the NEMS the stable energy minimum is the case $y = 0$, which is maintained as long as $y_* < 1/3$. Interestingly, the NEMS energy landscape is the flipped version of that in Fig. 2. At $y_* = 1/3$, the pull-in condition is reached and the system is no longer stable, causing the air-gap to collapse through phase transition.

If a regular dielectric capacitor is placed in series with the NEMS (or MEMS) capacitor, then the system can reversibly and reliably (phase) transition between pull-in and pull-out states. The states are distinguished by the order parameter, $y(V)/y_0$ [29]. These voltage-tunable, non-linear, hysteretic PT capacitors have been used as variable-frequency filters for radio frequency (RF) circuits [30]. Another interesting application of NEMS is the interferometric modulator display (i.e., mirasol display), where each pixel is made of an independently addressable, voltage-tunable NEMS capacitor. The voltage-controlled airgap defines the pixel color (i.e., structure color), making it possible to create "zero-hold-energy" full-color display for mobile phones or other energy-constrainted devices.

When a MEMS structure is integrated with the gate stack of a MOSFET, one obtains an important class of PT switches called the **Suspended-Gate FET (SGFET)**. It will become

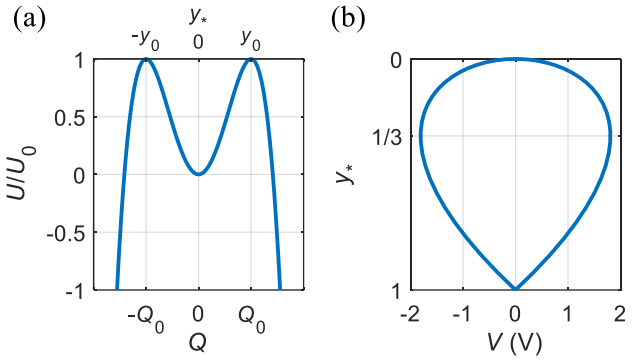

FIGURE 5. (a) NEMS energy landscape at equilibrium ($V = 0$). U is normalized by the maximum value obtained at $Q = \pm Q_0$, or, equivalently, $y = y_0$. (b) $y_* - V$ plot showing that the air-gap collapses for $y_* > y_c$ which is called the pull-in condition.

clearer from the discussion of the NCFET (which embeds a ferroelectric material in the gate stack of a regular MOSFET) that the SGFET reduces the sub-threshold slope below the Boltzmann limit [29]. SGFET can also be used as a memory element [31] or as a highly sensitive nanocantilever biosensor that beats the Nernst limit [13].

B. Phase transition in NCFET for logic applications

Negative capacitance field-effect transistor (NCFET) is a class of steep-slope transistors that integrate a ferroelectric insulator (e.g., HfO_2) in the gate stack of a regular MOSFET [5], [32], as sketched in Fig. 6(a).

The physics of a ferroelectric capacitor reducing $S < S_{\rm BT} \approx 60\,{\rm mV/dec}$ at room temperature can be explained by the circuit schematic in Fig. 6(b). The circuit represents the gate stack of the NCFET at the source side [33] so that we can relate the applied gate-to-source bias ($V_{\rm GS}$) and the surface potential ($\psi_{\rm s}$), i.e.,

$$V_{\rm GS} - V_{\rm FB} = V_{\rm FE} + V_{\rm INT} = V_{\rm FE} + V_{\rm ox} + \psi_{\rm s}, \tag{8}$$

where $V_{\rm FB}$ is the flat-band voltage, $V_{\rm FE}$ is the voltage drop across the ferroelectric layer, $V_{\rm INT}$ is the internal potential of the MOSFET, and $V_{\rm ox}$ is the voltage drop across the gate insulator (e.g., SiO_2). $V_{\rm FE}$ is determined through the so-called Landau-Khalatnikov equation [5], which expresses the dynamic behavior of ferroelectric.

Therefore (in one dimension, at steady-state, and neglecting terms of higher order than 4),

$$\frac{\partial U}{\partial P} = 0 \tag{9a}$$

$$U = \alpha P^2 + \beta P^4 - E_{\rm FE}\cdot P \tag{9b}$$

$$V_{\rm FE} = E_{\rm FE} t_{\rm FE} = t_{\rm FE}(2\alpha P + 4\beta P^3), \tag{9c}$$

where P is the ferroelectric polarization, $\alpha = \alpha_0(T - T_C)$ (T_C is the Curie temperature [27]), β is a temperature independent parameter, and $t_{\rm FE}$ is the ferroelectric layer thickness (Eq. (9c) is obtained by combining Eqs. (9a) and (9b)). At room temperature $\alpha < 0$ so that the energy landscape of the ferroelectric layer is essentially identical

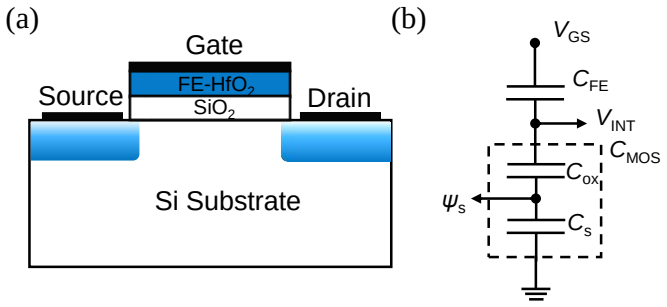

FIGURE 6. (a) Sketch of the NCFET that integrates a ferroelectric HfO2 layer in the gate stack of a regular MOSFET (for clarity here we considered a planar MOSFET, but the concept can be applied also to FinFET and GAA-FET). (b) Simplified circuit schematic of the gate stack of the NCFET.

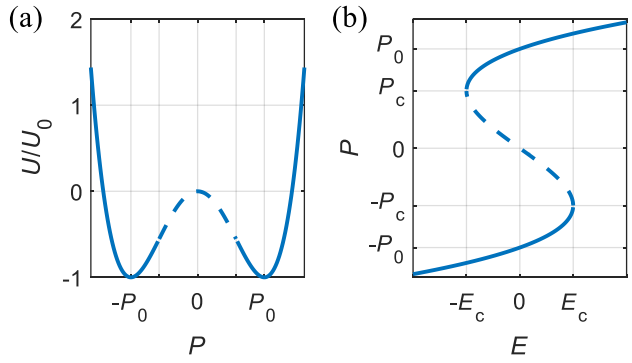

FIGURE 7. (a) NCFET energy landscape at equilibrium ($V_{\rm FE}=0$). U is normalized by the minimum value obtained at $P=\pm P_0$. (b) $P-E$ s-shaped plot showing the region of negative capacitance ($(\partial P/\partial V))^{-1}\equiv C_{\rm FE}<0$) with a dashed line (see also the corresponding energy in panel (a)). $P_{\rm c}$ ($E_{\rm c}$) are defined as the critical values at the boundaries of the unstable NC region.

to that of Fig. 2(b). For ferroelectrics, polarization P is the order parameter and temperature is the control parameter ($2^{\rm nd}$-order phase transition occurs for HfO_2). Eqs. (9b) and (9c) are plotted in Fig. 7.

The region denoted by the dashed line in Fig. 7(b) is the so-called negative capacitance region (because $(\partial P/\partial V)^{-1}\equiv C_{\rm FE}<0$), and it is an unstable region of operation for a free-standing ferroelectric layer. The reason why this region can be stabilized in an NCFET is that while locally the ferroelectric capacitance is negative, the total gate-to-source capacitance ($C_{\rm GS}^{-1}=C_{\rm FE}^{-1}+C_{\rm MOS}^{-1}$) is positive.

The negative capacitance provides internal voltage amplification because the potential energy stored by the ferroelectric when stabilized in one of the two minima, see Fig. 7(a), is released. If we define the voltage amplification as

$$A_{\rm V}\equiv\frac{\partial V_{\rm INT}}{\partial V_{\rm GS}}=\frac{|C_{\rm FE}|}{|C_{\rm FE}|-C_{\rm MOS}}>1, \qquad (10)$$

then the body factor of the NCFET defined as $m'\equiv(\partial\psi_s/\partial V_{\rm GS})^{-1}$ can be written as $m'=m/A_V<m$ (m is that of the underlying MOSFET, defined in Appendix A). The reduction of body factor paves the way for a design space that achieves $S<S_{\rm BT}$. The design space for

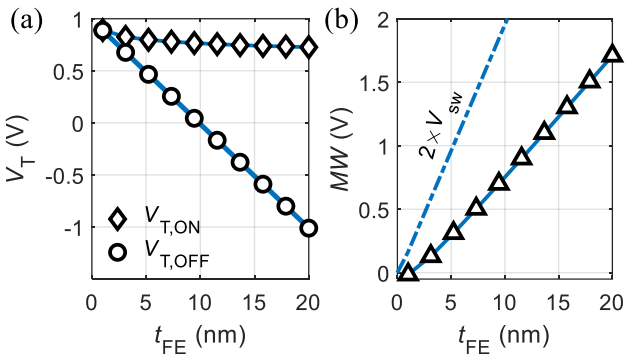

FIGURE 8. Dependence on ferroelectric thickness ($t_{\rm FE}$) of (a) ON- ($V_{\rm T,ON}$) and OFF-threshold voltage ($V_{\rm T,OFF}$), and (b) memory window (MW). While $V_{\rm T,ON}$ weakly depends on $t_{\rm FE}$, $V_{\rm T,OFF}$ (and consiquently, MW) varies linearly with $t_{\rm FE}$ through $V_{\rm sw}$ (defined in the text). In (b), the line $2\times V_{\rm sw}=E_{\rm c}t_{\rm FE}$ ($E_{\rm c}$ is the critical ferroelectric field) represents the $MW_{\rm MAX}-t_{\rm FE}$ curve.

stable operation in the negative capacitance is defined by the following,

$$C_{\rm MOS}<|C_{\rm FE}|<C_{\rm ox}, \qquad (11)$$

that is derived by setting the constraints $C_{\rm GS}>0$ and $m<1$ ($C_{\rm ox}$ is the gate oxide capacitance).

C. Phase transition in Ferroelectric Memory Transistor

If the condition is $C_{\rm MOS}<|C_{\rm FE}|$ violated, then the NCFET enters the so-called 'hysteretic' regime which exhibits ultra-steep switching and two separate threshold voltages: this is the operating regime of FeFETs. FeFETs bear the same structure as that of NCFETs, i.e., with a ferroelectric layer inserted in the gate stack between the metal contact and the oxide layer. However, the thickness of the ferroelectric layer is chosen to de-stabilize device operation around the negative capacitance region, causing abrupt switching and hysteresis. More specifically, when the field across the ferroelectric layer approaches $E_{\rm c}$ ($-E_{\rm c}$) (see Fig. 7(b)) and polarization is negative (positive) then the operating point jumps immediately to guarantee positive (negative) polarization to stabilize the gate capacitance (i.e., to guarantee that $C_{\rm GS}>0$) [33].

The abrupt transition can also be understood with the aid of Fig. 7(a); if the ferroelectric is biased such that the energy of one stable energy minimum is raised and the energy barrier reduced sufficiently, then abrupt switching to the opposite state occurs (in the NCFET this transition is smoothed by flattening of the negative capacitance region obtained when Eq. (11) is satisfied [34]).

FeFETs can be used as non-volatile memory devices because they retain their "memory" state even without applied bias. Since the two states are separated by energy barrier, i.e., it is necessary to apply different (positive or negative) bias values to induce switching from one state to the other. Depending on the polarization state of the gate capacitor, the FEFET has two different threshold voltages. The difference of these two threshold voltages is known as the memory window (MW).

A closed-form expression for $MW = V_{\mathrm{T,ON}} - V_{\mathrm{T,OFF}}$ can be derived for a planar FeFET assuming that at switching conditions the semiconductor charge necessary to screen the polarization charge is composed solely of inversion charge [35]. A number of papers in the literature report - by means of either experimental findings [36] or numerical simulations [37] - that a significant fraction of the polarization charge is screened by trapped charge either in the dielectric layer or at the dielectric/ferroelectric interface, with concentrations in the range of $10^{13} - 10^{14}\mathrm{cm}^{-2}$ [36], [38]. Here, for the sake of argument, we consider only the fraction of polarization charge screened by the inversion layer charge. By following the procedure outlined in [35] one obtains

$$V_{\mathrm{T,ON}} = V_{\mathrm{FB}} - 2V_{\mathrm{TH}} + 2V_{\mathrm{TH}} \ln\left(-\frac{2V_{\mathrm{TH}}}{aQ_0}\right) \tag{12a}$$

$$V_{\mathrm{T,OFF}} = V_{\mathrm{FB}} - V_{\mathrm{sw}} + 2V_{\mathrm{TH}} \ln\left(\frac{Q_{\mathrm{sw}}}{Q_0}\right) \tag{12b}$$

$$MW = -2V_{\mathrm{TH}} + V_{\mathrm{sw}} + \left[2V_{\mathrm{TH}} \ln\left(\frac{4}{3}\frac{V_{\mathrm{TH}}}{V_{\mathrm{sw}}}\right)\right], \tag{12c}$$

where $V_{\mathrm{TH}} = k_{\mathrm{B}}T/q$ is the thermal voltage (k_{B} is the Boltzmann constant, T is the temperature, and q is the elementary charge), $Q_0 = \sqrt{2\varepsilon_{\mathrm{s}} q V_{\mathrm{TH}} n_{\mathrm{i}}^2 / N_{\mathrm{A}}}$ (ε_s is Si dielectric constant, n_{i} is the Si intrinsic carrier concentration and N_{A} the doping of the Si substrate), $V_{\mathrm{sw}} = (2/3)|a|\sqrt{|a|/3b}$ (with $a = 2\alpha t_{\mathrm{FE}} + 1/C_{\mathrm{ox}}$, and $b = 4\beta t_{\mathrm{FE}}$), and $Q_{\mathrm{sw}} = \sqrt{|a|/3b}$. In a first approximation, Eq. (12c) indicates that MW linearly depends on t_{FE} through V_{sw}, as expected since the voltage drop across the ferroelectric is simply $V_{\mathrm{FE}} = E_{\mathrm{FE}} t_{\mathrm{FE}}$. The MW of a FeFET is always less than $MW_{\max} = 2E_{\mathrm{c}} t_{\mathrm{FE}} = 2V_{\mathrm{sw}}$ as only a fraction of the applied voltage drops across the ferroelectric, see Fig. 8(b). Specifically, from Eq. (12c) one finds that $MW \propto V_{\mathrm{sw}}$ due to non-symmetric switching conditions.

D. Phase transition improves SNR of Nano biosensors

Nano biosensors based on semiconductor devices detect some quantity related to biomolecules (e.g. charge, mass, shape, etc.) and then convert them into a measurable electrical signal. The biological element to be measured can be the density of biomolecules, the pH of a substance, the charge carried by deoxyribonucleic acid (DNA) molecules, etc. In this context, biosensing involves an indirect type of measurement, where the quantity of interest is obtained from the actual measured electrical quantity via well-known physical relations depending on the detection mechanism. Here we discuss two kinds of biosensors that can exploit features of phase transition elements to improve their signal-to-noise ratio (SNR). The devices under investigation are the negative capacitance ion-sensitive field effect transistor (NC-ISFET, i.e., a potentiometric nanobiosensor) [39]and the flexure sensitive field effect transistor (FlexureFET, i.e., a nano-cantilever biosensor) [13], and .

1) NC-ISFET improves SNR of a biosensor

An NC-ISFET is the combination of a NCFET with an Ion-Selective FET (ISFET), the latter being a MOSFET with the gate contact realized by a reference electrode placed in an aqueous solution in contact with the gate insulator. In an NC-ISFET conversely, it is the ferroelectric layer that is in contact with the aqueous solution [39], [40], see Fig. 9(a). ISFET is sensitive to the *charge* of the solution determined by the presence of salt in the solution itself that makes it an electrolyte, i.e., a medium containing positive (H^+) and negative (OH^-) ions. These ions interact with the top surface of the gate insulator layer via its dangling bonds (forming OH amphoteric sites, called receptors) through protonation/deprotonation reactions that effectively allow measuring the pH of the solution. ISFET is able to sense the charge related to pH because the charge of the electrolyte is screened by the semiconductor charge, namely,

$$Q_{\mathrm{s}} + Q_{\mathrm{surf}} + Q_{\mathrm{dl}} = 0, \tag{13}$$

where Q_{s} is the semiconductor charge, Q_{surf} is the surface charge due to the exchange of ions, and Q_{dl} is the so-called double-layer charge. The double-layer charge is due to the accumulation of ions at the electrolytic/insulator interface that limits the further accumulation of ions [41] (akin to the inversion layer in the MOSFET, that limits the increase of surface potential above threshold [42]). The presence of Q_{dl} limits the sensitivity of a regular ISFET to the so-called Nernst limit of $S_N \approx 60\,\mathrm{mV/pH}$ at room temperature [43]. Instead, an NC-ISFET can go beyond this limit due to the voltage amplification effect given by the negative capacitance of the ferroelectric layer [39].

Q_{surf} can be analytically related to the pH of the solution by the site-binding model, while Q_{dl} is determined by solving the Poisson-Boltzmann equation in the electrolyte [43]. By assuming that most of Q_{surf} is screened by Q_{dl} (i.e., letting $Q_s \approx 0$ in Eq. (13)) then a compact model for the gate stack of the ISFET can be written as follows (valid in quasi-static conditions),

$$V_{\mathrm{GS}} = V_{\mathrm{FG}} + \psi_{\mathrm{e}} \tag{14a}$$

$$\psi_{\mathrm{e}} = 2V_{\mathrm{TH}} \sinh^{-1}\left(\frac{Q_{\mathrm{surf}}}{\sqrt{8kT\varepsilon_{\mathrm{w}} n_0}}\right) + \frac{Q_{\mathrm{surf}}}{C_{\mathrm{ST}}}, \tag{14b}$$

where $\varepsilon_{\mathrm{w}} \approx 80\varepsilon_0$ is the dielectric constant of water, $n_0 = N_{\mathrm{AVG}} \times i_0$ is the concentration of salt in the electrolyte (N_{AVG} is Avogadro's constant, i_0 is the molar concentration in $\mathrm{mol/L}$), and C_{ST} is the Stern-layer capacitance (accounting for the finite size of ions accumulating at the surface [43]). Eq. (14) simply states that ISFET works as an ordinary MOSFET whose V_{FB} (and thus the threshold voltage, V_{T}) is shifted rigidly depending on the pH of the sample solution. The dependence of V_{T} (and thus I_{D}) on pH can be visualized in Fig. 9(b). The internal voltage amplification of the NCFET improves sensitivity of the ISFET (defined as $S_{\mathrm{NCISFET}} \equiv I_{\mathrm{D},1}/I_{\mathrm{D},2}$) thanks to the reduction in body factor m, as explained in Section III.B. This is visualized in Fig. 9(c), showing the increase of

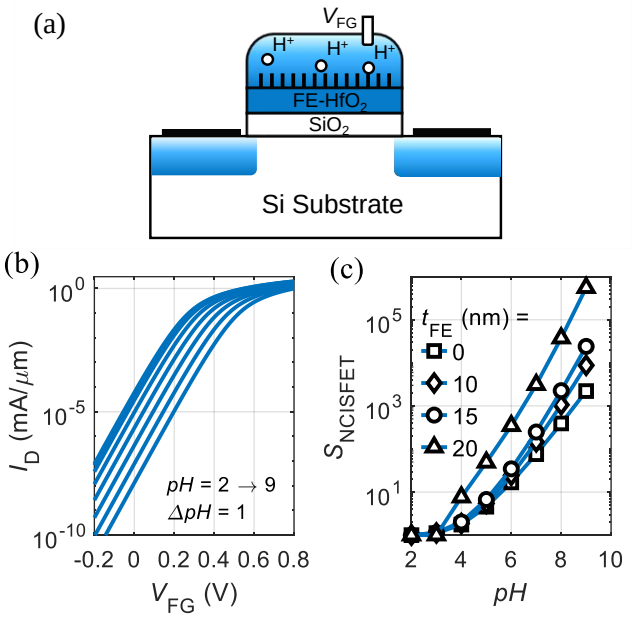

FIGURE 9. **(a) Sketch of the NC-ISFET cross-section. (b) $I-V$ curves of an ISFET with varying pH concentration of the electrolytic solution. V_T increases as pH increases. (c) Sensitivity of NC-ISFET for different ferroelectric layer thickness. As $|C_{\rm FE}|$ gets closer to $C_{\rm MOS}$ the voltage amplification increases and thus does sensitivity. ($t_{\rm FE}=0$ is the regular ISFET).**

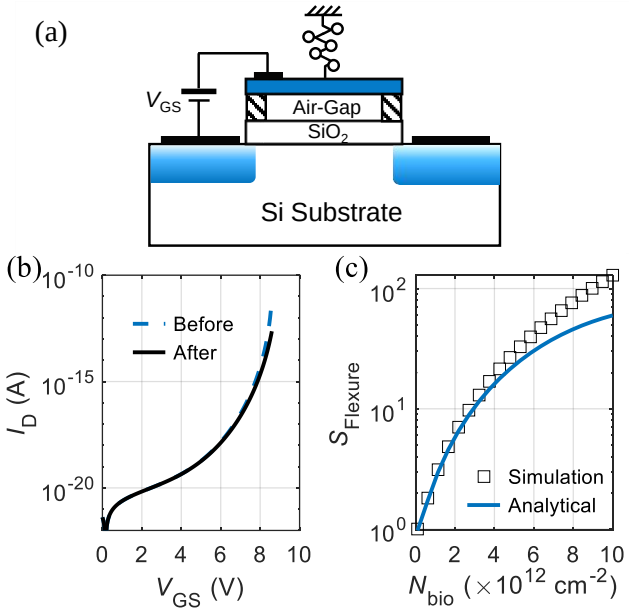

FIGURE 10. **(a) Sketch of the FlexureFET cross-section. (b) $I-V$ curve of the FlexureFET before and after capture or biomolecule. (c) Sensitivity of FlexureFET as a function of biomolecule concentration. Symbols denote the numerical simulation and solid line is Eq. (16).**

sensitivity with increasing $t_{\rm FE}$. This dependence is readily explained: as $t_{\rm FE}$ decreases, $|C_{\rm FE}|$ reduces and gets closer to $C_{\rm MOS}$, thus increasing A_V, see Eq. (10), and thus sensitivity increases. NC-ISFET improves not only sensitivity but also SNR due to reduction of flicker noise for increasing $t_{\rm FE}$ as the total gate capacitance of the device increases [39], [44].

2) FlexureFET is highly sensitive to the adsorbed biomolecules

FlexureFET is a nano biosensor based on the SGFET concept where the moving plate of the NEMS capacitor in the gate stack is sensitive to the presence of biomolecules, see Fig. 10(a). More specifically, sensing occurs because biomolocules attactred to the device vary the stiffness of the movable electrode, k. This variation is detected by the device as a variation of the transistor current. FlexureFET exhibits high sensitivity near pull-in condition because even a small variation in biomolecule concentration causes an exponential variation in transistor current [13]. This is because, at least in the sub-threshold regime, the semiconductor charge depends exponentially on the surface potential ($\psi_{\rm s}$) [45], therefore current ratio before and after capture of biomolecules is [13],

$$\frac{I_{\rm D,1}}{I_{\rm D,2}} \approx \exp\left(-\frac{\Delta\psi_{\rm s}}{V_{\rm TH}}\right) \approx \exp\left(-\frac{y\Delta k + k\Delta y}{V_{\rm TH}\varepsilon_{\rm s} q N_{\rm A} A}\right), \quad (15)$$

where $N_{\rm A}$ is the doping of the MOSFET body, and $\varepsilon_{\rm s}$ is the relative semiconductor dielectric constant. Eq. (15) is derived assuming that a biomolecule acts on the movable beam by deforming its thickness by $\Delta t = N_{\rm bio}V_{\rm bio}$, where $N_{\rm bio}$ is the areal concentration of captured biomolecules, leading in turn to a relative variation of stiffness $\Delta k/k = 3\Delta t/t$ ($k \propto ELt^3/W^3$, where E is the Young's modulus of the beam and L, t, W are its length, thickness and width, respectively). Finally, it can be shown that the sensor sensitivity (defined as $S_{\rm Flexure} \equiv I_{\rm D,1}/I_{\rm D,2}$) at pull-in can be expressed as [13],

$$S_{\rm Flexure} \approx \exp\left(c_1\sqrt{N_{\rm bio}} - c_2 N_{\rm bio}\right), \quad (16)$$

where c_1, and c_2 are constants depending on NEMS and MOSFET parameters. Fig. 10(b) shows the $I-V$ characteristics of the FlexureFET before and after the capture of a biomolecule, while Fig. 10(c) shows the sensitivity of the device calculated with Eq. (16) and with a numerical simulation that includes both depletion and inversion charge [13].

Deviation from the simulation occurs for higher gate voltage because Eq. (16) was derived considering only the effect of depletion charge to arrive at a closed-form expression for S_F [13]. At fixed $N_{\rm bio}$, S_F values are considerably higher than those reported for other kinds of electrical and mechanical nano biosensors (e.g., Si nanowires, resonance mode cantilevers, etc.) [13]. Interestingly, FlexureFET not only improves sensitivity, but near the pull-in instability also the signal-to-noise ratio (SNR) improves, thanks to the inherent feedback loop given by the electrostatic force counterbalancing the mechanical one, that reduces the influence of force and stiffness fluctuations [46].

IV. CONCLUSIONS AND OUTLOOK

This paper presents a tutorial review of Phase Transition Switches, a promising class of devices that could surpass the

Boltzmann limits in computing, storage, sensing, and display technologies. The defining feature of these devices is their double-well energy landscape, characterized by two stable operating points (corresponding to energy minima) separated by a barrier. This unique property enables enhancements to classical semiconductor devices, such as nonvolatility, steep switching, and noise rejection.

In this paper, we explained the fundamentals of phase transition physics through the simple example of a buckling stick, then applied this theory to novel devices like NEMS capacitors, negative capacitance transistors, ferroelectric transistors, and nanobiosensors. This unified framework not only simplifies the analysis of diverse devices but also inspires innovative uses of the energy landscape to develop entirely new types of devices, such as flexure FET biosensors.

The review omits several important topics. First, phase-transition switches present unique reliability challenges compared to Boltzmann switches, which require systematic exploration to identify failure mechanisms and develop mitigation strategies. For example, reduced speed and inefficient switching in ferroelectric memory switches have been linked to domain formation, interfacial defects, and grain boundaries. Addressing these issues will involve creating low-defect density phase-transition materials for future low-power semiconductor devices. Additionally, this review focuses on *non-volatile* bistable devices with states separated by an energy barrier. Future research should explore *volatile* bistable devices, such as SRAM memory, PhaseFETs, MottFETs, and Resonant-tunneling diodes, which operate with states separated by a *power* barrier. We will discuss these issues in a future article.

Appendix A

Boltzmann Limit and Subthreshold Slope of Transistors. A classical MOSFET allows or inhibits current flow by modulating an energy barrier. According to Boltzmann statistics, the probability of carriers to overcome the barrier is $\propto \exp(-E/k_{\mathrm{B}}T)$, where E is the energy barrier, k_{B} is the Boltzmann constant, and T is the temperature. This relationship not only establishes a minimum energy to ensure proper switching [45], [47], but it also sets the minimum switching slope, S, of semiconductor devices to $S_{\mathrm{BT}} \approx 60\,\mathrm{mV/dec}$. As a matter of fact, it can be shown that

$$S = \underbrace{\left(\frac{\partial \psi_{\mathrm{s}}}{\partial V_{\mathrm{GS}}}\right)^{-1}}_{m} \times \underbrace{\log(10) V_{\mathrm{TH}}}_{n}. \tag{17}$$

The body factor m expresses the fraction of applied bias that is transferred to the surface potential (and thus to the semiconductor). The transport factor n is limited by Boltzmann statistics (S_{BT} and is obtained from Eq. (17) by letting $m = 1$). This fundamental limit, also known as 'Boltzmann Tyranny', has slowed down transistor scaling because the off-state current, I_{OFF}, is related to the threshold voltage, V_{T}, and S, i.e., $I_{\mathrm{OFF}} \propto e^{-qV_{\mathrm{T}}/mk_{\mathrm{B}}T} = 10^{-V_{\mathrm{T}}/S}$ [48].

Since n depends on the physics of the transport mechanism below threshold (i.e., thermionic emission of carriers over the energy barrier), the only way to enable steep-slope switching is to obtain $m < 1$. SGFET and NCFET have $m < 1$ due to the concept of negative capacitance. For SGFET, this occurs under pull-in conditions [29], whereas for NCFET, it occurs in the negative capacitance region [33]. Unfortunately, both devices achieve steep slope operation only for a limited bias range. Interestingly, it is possible to increase the operating voltage range using a series combination of ferromagnetic and antiferroelectric layers [49], or by combining the SGFET with the NCFET in a single device [50].

Appendix B

Nernst limits and sensitivity limits of biosensors. A similar expression to Eq. (17) can be obtained for ISFET sensitivity, i.e.,

$$S_{\mathrm{V}} = \underbrace{\left[\frac{1}{\frac{1}{C_{\mathrm{surf}}}(C_{\mathrm{diff}} + C_{\mathrm{MOS}}) + 1}\right]}_{m} \times \underbrace{\ln(10) V_{\mathrm{TH}}}_{n} \tag{18}$$

where C_{surf}, C_{diff} are parameters specific to the sensor itself [51]. Again, m is related to the modulation efficiency of the semiconductor potential by the gate bias, whereas n is determined by the physics of biomolecules detection in this case. By letting $m = 1$ in Eq. (18) we obtained the so-called Nernst-limit. NC-ISFET beats the Nernst limit thanks to the increased C_{MOS} obtained with the negative capacitance [39].

ACKNOWLEDGMENTS

The authors acknowledge the following students and colleagues for their contribution to many of the topics covered in this paper: Muhammad Masuduzzaman, Ankit Jain, Pradeep Nair, Piyush Dak, Kamal Karda, Sayeef Salahuddin, Suman Datta, Supryo Datta, Peide D. Ye, and Mark Lundstrom.

REFERENCES

[1] M. S. Lundstrom and M. A. Alam, "Moore's law: The journey ahead," *Science*, vol. 378, no. 6621, pp. 722–723, 2022. DOI:10.1126/science.ade2191

[2] I. I. R. for Devices and Systems, "Beyond CMOS and Emerging Materials Integration," *Institute of Electrical and Electronics Engineers (IEEE)*, 2023. DOI:10.60627/0P45-ZJ55

[3] M. Masuduzzaman and M. A. Alam. IEEE EDS Newsletter (October 2016). [Online]. Available: https://eds.ieee.org/images/files/newsletters/newsletter_oct16.pdf

[4] J. C. Wong and S. Salahuddin, "Negative capacitance transistors," *Proceedings of the IEEE*, vol. 107, no. 1, pp. 49–62, Jan. 2019. DOI:10.1109/JPROC.2018.2884518

[5] S. Salahuddin and S. Datta, "Use of negative capacitance to provide voltage amplification for low power nanoscale devices," *Nano Letters*, vol. 8, no. 2, pp. 405–410, 2008. DOI:10.1021/nl071804g

[6] A. Peschot, C. Qian, and T.-J. Liu, "Nanoelectromechanical switches for low-power digital computing," *Micromachines*, vol. 6, no. 8, pp. 1046–1065, Aug. 2015. DOI:10.3390/mi6081046

[7] H. Kam, D. Lee, R. Howe, and T.-J. King, "A new nano-electro-mechanical field effect transistor (NEMFET) design for low-power electronics," in *IEEE InternationalElectron Devices Meeting*, Dec. 2005, pp. 463–466. DOI:10.1109/IEDM.2005.1609380

[8] T. Sakamoto, H. Sunamura, H. Kawaura, T. Hasegawa, T. Nakayama, and M. Aono, "Nanometer-scale switches using copper sulfide," *Applied Physics Letters*, vol. 82, no. 18, pp. 3032–3034, May 2003. DOI:10.1063/1.1572964

[9] H. Takagi and H. Y. Hwang, "An Emergent Change of Phase for Electronics," *Science*, vol. 327, no. 5973, pp. 1601–1602, Mar. 2010. DOI:10.1126/science.1182541

[10] B. Comiskey, J. D. Albert, H. Yoshizawa, and J. Jacobson, "An electrophoretic ink for all-printed reflective electronic displays," *Nature*, vol. 394, no. 6690, pp. 253–255, Jul. 1998. DOI:10.1038/28349

[11] D. Graham-Rowe, "Electronic paper targets colour video," *Nature Photonics*, vol. 2, no. 4, pp. 204–205, Apr. 2008. DOI:10.1038/nphoton.2008.38

[12] J. Chen, W. Cranton, and M. Fihn, Eds., *Handbook of Visual Display Technology*. Springer Cham, 2016.

[13] A. Jain, P. R. Nair, and M. A. Alam, "Flexure-FET biosensor to break the fundamental sensitivity limits of nanobiosensors using nonlinear electromechanical coupling," *Proceedings of the National Academy of Sciences*, vol. 109, no. 24, pp. 9304–9308, 2012. DOI:10.1073/pnas.1203749109

[14] V. Kumar, J. W. Boley, Y. Yang, H. Ekowaluyo, J. K. Miller, G. T.-C. Chiu, and J. F. Rhoads, "Bifurcation-based mass sensing using piezoelectrically-actuated microcantilevers," *Applied Physics Letters*, vol. 98, no. 15, p. 153510, Apr. 2011. DOI:10.1063/1.3574920

[15] W. Zhang and K. L. Turner, "Application of parametric resonance amplification in a single-crystal silicon micro-oscillator based mass sensor," *Sensors and Actuators A: Physical*, vol. 122, no. 1, pp. 23–30, Jul. 2005. DOI:10.1016/j.sna.2004.12.033

[16] L. D. Forest, "The audion; a new receiver for wireless telegraphy," *Transactions of the American Institute of Electrical Engineers*, vol. XXV, pp. 735–763, 1906. DOI:10.1109/T-AIEE.1906.4764762

[17] O. Lossev, "Cii. luminous carborundum detector and detection effect and oscillations with crystals," *The London, Edinburgh, and Dublin Philosophical Magazine and Journal of Science*, vol. 6, no. 39, pp. 1024–1044, 1928. DOI:10.1080/14786441108564683

[18] J. Bardeen and W. H. Brattain, "The transistor, a semiconductor triode," *Phys. Rev.*, vol. 74, pp. 230–231, Jul 1948. DOI:10.1103/PhysRev.74.230

[19] I. M. Ross, "Semiconductive translating device," US Patent US2 791 760A, May, 1957.

[20] M. M. Atalla, E. Tannenbaum, and E. J. Scheibner, "Stabilization of silicon surfaces by thermally grown oxides," *The Bell System Technical Journal*, vol. 38, no. 3, pp. 749–783, 1959. DOI:10.1002/j.1538-7305.1959.tb03907.x

[21] P. Bergveld, "Development of an ion-sensitive solid-state device for neurophysiological measurements," *IEEE Transactions on Biomedical Engineering*, vol. BME-17, no. 1, pp. 70–71, 1970. DOI:10.1109/TBME.1970.4502688

[22] D. M. Newns, J. A. Misewich, C. C. Tsuei, A. Gupta, B. A. Scott, and A. Schrott, "Mott transition field effect transistor," *Applied Physics Letters*, vol. 73, no. 6, pp. 780–782, 08 1998. DOI:10.1063/1.121999

[23] A. Ionescu, V. Pott, R. Fritschi, K. Banerjee, M. Declercq, P. Renaud, C. Hibert, P. Fluckiger, and G. Racine, "Modeling and design of a low-voltage soi suspended-gate mosfet (sg-mosfet) with a metal-over-gate architecture," in *Proceedings International Symposium on Quality Electronic Design*, 2002, pp. 496–501. DOI:10.1109/ISQED.2002.996794

[24] K. Akarvardar, D. Elata, R. Parsa, G. C. Wan, K. Yoo, J. Provine, P. Peumans, R. T. Howe, and H.-S. P. Wong, "Design considerations for complementary nanoelectromechanical logic gates," in *2007 IEEE International Electron Devices Meeting*, 2007, pp. 299–302. DOI:10.1109/IEDM.2007.4418930

[25] N. Shukla, A. V. Thathachary, A. Agrawal, H. Paik, A. Aziz, D. G. Schlom, S. K. Gupta, R. Engel-Herbert, and S. Datta, "A steep-slope transistor based on abrupt electronic phase transition," *Nature Communications*, vol. 6, no. 1, p. 7812, Aug. 2015. DOI:10.1038/ncomms8812

[26] R. V. Solé, *Phase Transitions*. Princeton University Press, 2011.

[27] P. Chandra and P. B. Littlewood, "A Landau Primer for Ferroelectrics," in *Physics of Ferroelectrics - A Modern Perspective*, 1st ed., K. M. Rabe, C. H. Ahn, and J.-M. Triscone, Eds. New York: Springer, 2007, vol. 105, ch. 3, pp. 69–116.

[28] M. Masuduzzaman and M. A. Alam, "Effective nanometer airgap of NEMS devices using negative capacitance of ferroelectric materials," *Nano Letters*, vol. 14, no. 6, pp. 3160–3165, 6 2014. DOI:10.1021/nl5004416

[29] A. Jain and M. A. Alam, "Prospects of hysteresis-free abrupt switching (0 mV/decade) in landau switches," *IEEE Transactions on Electron Devices*, vol. 60, no. 12, pp. 4269–4276, 12 2013. DOI:10.1109/TED.2013.2286997

[30] D. Peroulis, S. Pacheco, K. Sarabandi, and L. Katehi, "Electromechanical considerations in developing low-voltage rf mems switches," *IEEE Transactions on Microwave Theory and Techniques*, vol. 51, no. 1, pp. 259–270, 2003. DOI:10.1109/TMTT.2002.806514

[31] D. Molinero, N. Abele, L. Castaner, and A. Ionescu, "Oxide charging and memory effects in suspended-gate fet," in *2008 IEEE 21st International Conference on Micro Electro Mechanical Systems*, 2008, pp. 685–688. DOI:10.1109/MEMSYS.2008.4443749

[32] M. A. Alam, M. Si, and P. D. Ye, "A critical review of recent progress on negative capacitance field-effect transistors," *Applied Physics Letters*, vol. 114, no. 9, 2019. DOI:10.1063/1.5092684

[33] G. Pahwa, T. Dutta, A. Agarwal, S. Khandelwal, S. Salahuddin, C. Hu, and Y. S. Chauhan, "Analysis and Compact Modeling of Negative Capacitance Transistor with High ON-Current and Negative Output Differential Resistance - Part I: Model Description," *IEEE Transactions on Electron Devices*, vol. 63, no. 12, pp. 4981–4985, 12 2016. DOI:10.1109/TED.2016.2614432

[34] N. Zagni and M. A. Alam, "Reliability Physics of Ferroelectric/Negative Capacitance Transistors for Memory/Logic Applications: An Integrated Perspective," *Journal of Materials Research*, pp. 1–11, 2021. DOI:10.1557/s43578-021-00420-1

[35] H. P. Chen, V. C. Lee, A. Ohoka, J. Xiang, and Y. Taur, "Modeling and design of ferroelectric MOSFETs," *IEEE Transactions on Electron Devices*, vol. 58, no. 8, pp. 2401–2405, 8 2011. DOI:10.1109/TED.2011.2155067

[36] K. Toprasertpong, M. Takenaka, and S. Takagi, "Direct observation of interface charge behaviors in fefet by quasi-static split c-v and hall techniques: Revealing fefet operation," in *2019 IEEE International Electron Devices Meeting (IEDM)*, 2019, pp. 23.7.1–23.7.4. DOI:10.1109/IEDM19573.2019.8993664

[37] R. Fontanini, M. Segatto, M. Massarotto, R. Specogna, F. Driussi, M. Loghi, and D. Esseni, "Modeling and design of ftjs as multi-level low energy memristors for neuromorphic computing," *IEEE Journal of the Electron Devices Society*, vol. 9, pp. 1202–1209, 2021. DOI:10.1109/JEDS.2021.3120200

[38] S. Deng, Z. Jiang, S. Dutta, H. Ye, W. Chakraborty, S. Kurinec, S. Datta, and K. Ni, "Examination of the interplay between polarization switching and charge trapping in ferroelectric fet," in *2020 IEEE International Electron Devices Meeting (IEDM)*, 2020, pp. 4.4.1–4.4.4. DOI:10.1109/IEDM13553.2020.9371999

[39] N. Zagni, P. Pavan, and M. A. Alam, "Two-dimensional MoS2 negative capacitor transistors for enhanced (super-Nernstian) signal-to-noise performance of next-generation nano biosensors," *Applied Physics Letters*, vol. 114, no. 23, p. 233102, 6 2019. DOI:10.1063/1.5097828

[40] F. Bellando, C. K. Dabhi, A. Saeidi, C. Gastaldi, Y. S. Chauhan, and A. M. Ionescu, "Subthermionic negative capacitance ion sensitive field-effect transistor," *Applied Physics Letters*, vol. 116, no. 17, p. 173503, 2020. DOI:10.1063/5.0005411

[41] P. R. Nair and M. A. Alam, "Screening-limited response of nanobiosensors," *Nano Letters*, vol. 8, no. 5, pp. 1281–1285, 2008. DOI:10.1021/nl072593i

[42] Y. Taur and T. H. Ning, *Fundamentals of Modern VLSI Devices*. Cambridge University Press, 2009.

[43] P. Dak, W. Seo, B. Jung, and M. A. Alam, "A physics-based (Verilog-A) compact model for DC, quasi-static transient, small-signal, and noise analysis of MOSFET-based pH sensors," *IEEE Transactions on Electron Devices*, vol. 64, no. 3, pp. 1277–1285, 3 2017. DOI:10.1109/TED.2017.2651905

[44] S. Alghamdi, M. Si, L. Yang, and P. D. Ye, "Low frequency noise in MoS_2 negative capacitance field-effect transistor," in *IEEE International Reliability Physics Symposium (IRPS)*, 3 2018, pp. P–TX.1–1–P–TX.1–5. DOI:10.1109/IRPS.2018.8353696

[45] M. Lundstrom, *Fundamentals of Nanotransistors*. World Scientific, Sep. 2015.

[46] A. Jain and M. A. Alam, "Intrinsic low pass filtering improves signal-to-noise ratio in critical-point flexure biosensors," *Applied Physics Letters*, vol. 105, no. 8, p. 084106, 8 2014. DOI:10.1063/1.4893597

[47] V. Zhirnov, R. Cavin, J. Hutchby, and G. Bourianoff, "Limits to binary logic switch scaling - a gedanken model," *Proceedings of the IEEE*, vol. 91, no. 11, pp. 1934–1939, Nov. 2003. DOI:10.1109/JPROC.2003.818324

[48] C. C. Hu, *Modern Semiconductor Devices for Integrated Circuits*. Pearson, Mar. 2009.

[49] K. Karda, A. Jain, C. Mouli, and M. A. Alam, "An anti-ferroelectric gated landau transistor to achieve sub-60 mV/dec switching at low voltage and high speed," *Applied Physics Letters*, vol. 106, no. 16, p. 163501, 2015. DOI:10.1063/1.4918649

[50] A. Jain and M. A. Alam, "Proposal of a hysteresis-free zero subthreshold swing field-effect transistor," *IEEE Transactions on Electron Devices*, vol. 61, no. 10, pp. 3546–3552, Oct. 2014. DOI:10.1109/TED.2014.2347968

[51] P. Dak, P. Nair, J. Go, and M. A. Alam, "Extended-gate biosensors achieve fluid stability with no loss in charge sensitivity," *Device Research Conference - Conference Digest, DRC*, vol. 20, no. 2003, pp. 105–106, 2013. DOI:10.1109/DRC.2013.6633815